Electronic Supplementary Information (ESI)

Synergistic effect of graphene as a co-catalyst for enhanced daylight-induced photocatalytic activity of $Zn_{0.5}Cd_{0.5}S$ synthesized *via* an improved one-pot co-precipitation-hydrothermal strategy

Wee-Jun Ong,[a] Jia-Jun Yeong,[a] Lling-Lling Tan,[a] Boon Tong Goh,[b] Siek-Ting Yong,[a] Siang-Piao Chai[a,]*

[a] *Multidisciplinary Platform of Advanced Engineering, Chemical Engineering Discipline, School of Engineering, Monash University, Jalan Lagoon Selatan, Bandar Sunway, 47500 Selangor, Malaysia.*

[b] *Low Dimensional Materials Research Centre, Department of Physics, Faculty of Science, University of Malaya, 50603 Kuala Lumpur, Malaysia.*

* Corresponding author.

Tel: +603-5514 6234; Fax: +603-5514 6207

E-mail address: chai.siang.piao@monash.edu (S.-P. Chai)

(1) Preparation of graphene oxide (GO)

Graphite oxide was synthesized by modified Hummers' method through oxidation of graphite powder.[1,2] In detail, 3 g of graphite powder was added into an 80 ^{o}C mixture containing 12 mL of concentrated H_2SO_4, 2.5 g of P_2O_5 and 2.5 g of $K_2S_2O_8$. The mixture was stirred for 4.5 h at 80 ^{o}C. The mixture was then cooled to room temperature and diluted with 500 mL of DI water. Successively, the mixture was filtered and washed with DI water until the pH of the filtrate water became neutral. The product was then dried at 70 ^{o}C in an oven overnight. This pre-oxidized graphite was then dispersed into 120 mL of cold (0 ^{o}C) concentrated H_2SO_4. After that, 15 g of $KMnO_4$ was gradually added under stirring and the temperature of the mixture was kept below 20 ^{o}C by cooling. This resulted in the formation of a thick dark green paste. Successively, the mixture was stirred for 2 h at room temperature followed by diluting with 250 mL of DI water in an ice bath to keep the temperature below 50 ^{o}C. After another 2 h of stirring, the dark brownish solution was further diluted with 700 mL of DI water. Subsequently, 20 mL of H_2O_2 was slowly added into the mixture and a brilliant yellow product was formed along with bubbling. The mixture was then filtered and washed with 1 L of HCl to remove metal ions followed by 1 L of DI water to remove the acid. The filter cake was dispersed in water by mechanical agitation. Low speed centrifugation was performed at 1000 rpm for 2 min. The supernatant underwent high speed centrifugation steps at 10000 rpm for 30 min to remove small pieces of GO and water soluble by-products. Finally, the sediment was dried in air at 60 ^{o}C for 24 h. The graphite oxide product was ground into powder. To obtain GO sheets, a measured amount of graphite oxide was dispersed in deionized water and subjected to ultrasonication for 1 h at 40 kHz and 180 W using a table-top ultrasonic cleaner. The schematic diagram of the synthesis of GO sheets is shown in Fig. S1.

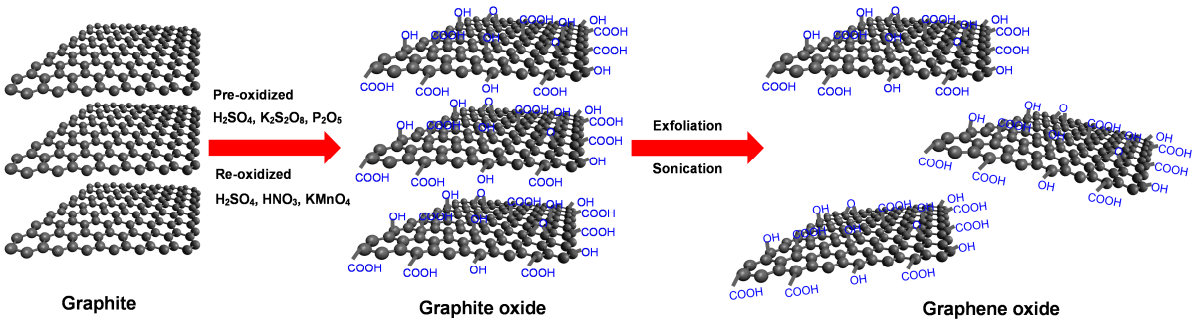

Fig. S1 Schematic illustration of the overall steps used in the preparation of GO sheets *via* modified Hummers' method.

(2) Photocatalytic degradation of Reactive black 5 (RB5) using pristine $Zn_xCd_{1-x}S$ nanocomposites

Fig. S2 depicts the photocatalytic degradation of RB5 over pristine $Zn_xCd_{1-x}S$. The initial studies showed that pristine $Zn_xCd_{1-x}S$ with x = 0.5 presented the highest degradation efficiency of RB5 (92.0%) with a corresponding rate constant, k of 0.0432 min^{-1}. This stoichiometry was chosen in the present work to examine the optimal condition of mass ratio of reduced graphene oxide (RGO) to $Zn_{0.5}Cd_{0.5}S$ for the RB5 photodegradation. For comparison, the commercially available photocatalyst P25 (Aeroxide) was used as the reference. It was found that the percentage of RB5 degradation obtained for $Zn_{0.5}Cd_{0.5}S$ was significantly higher (*ca*. 92 times) than that determined for the benchmark commercial P25. Therefore, this demonstrates that $Zn_{0.5}Cd_{0.5}S$-based composite is a superior visible-light photocatalyst for RB5 degradation.

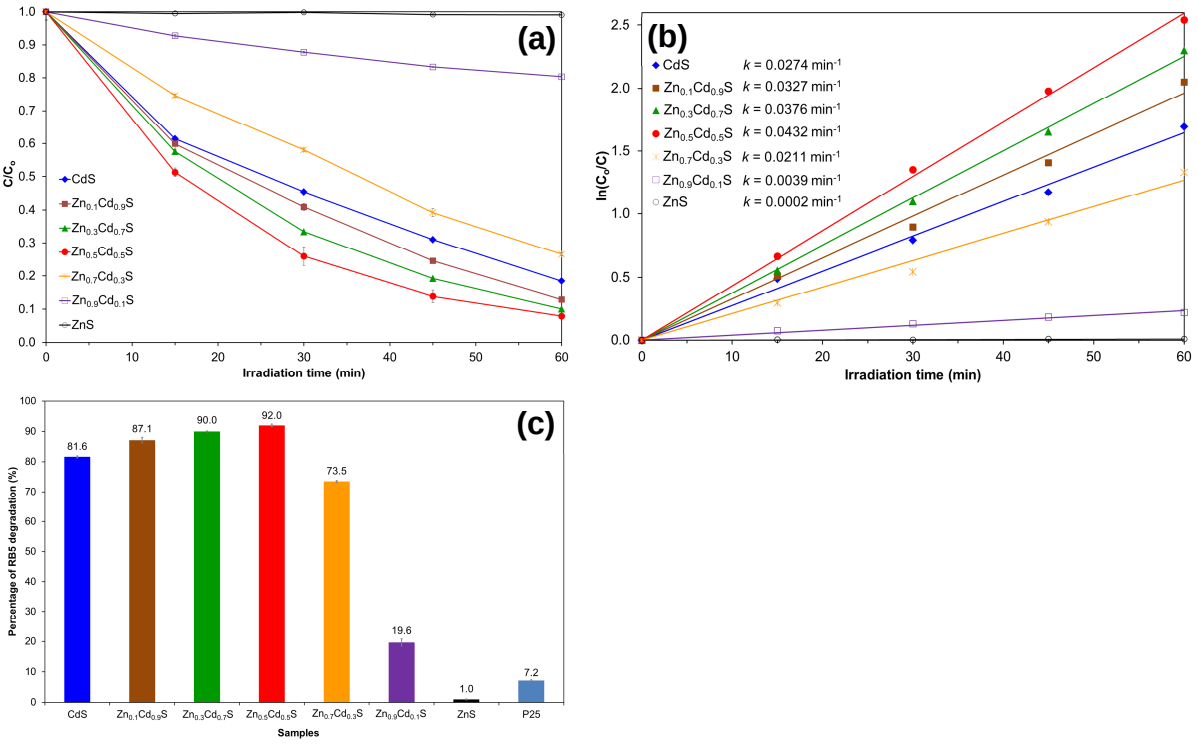

Fig. S2 (a) Photocatalytic degradation of RB5 over pristine $Zn_xCd_{1-x}S$ under visible light irradiation. (b) Pseudo first order kinetic reaction of RB5 degradation under visible light irradiation. (c) Percentage of RB5 degradation for the samples after 60 min irradiation with visible light.

(3) Morphology and particle size analysis of the studied photocatalysts as control experiments

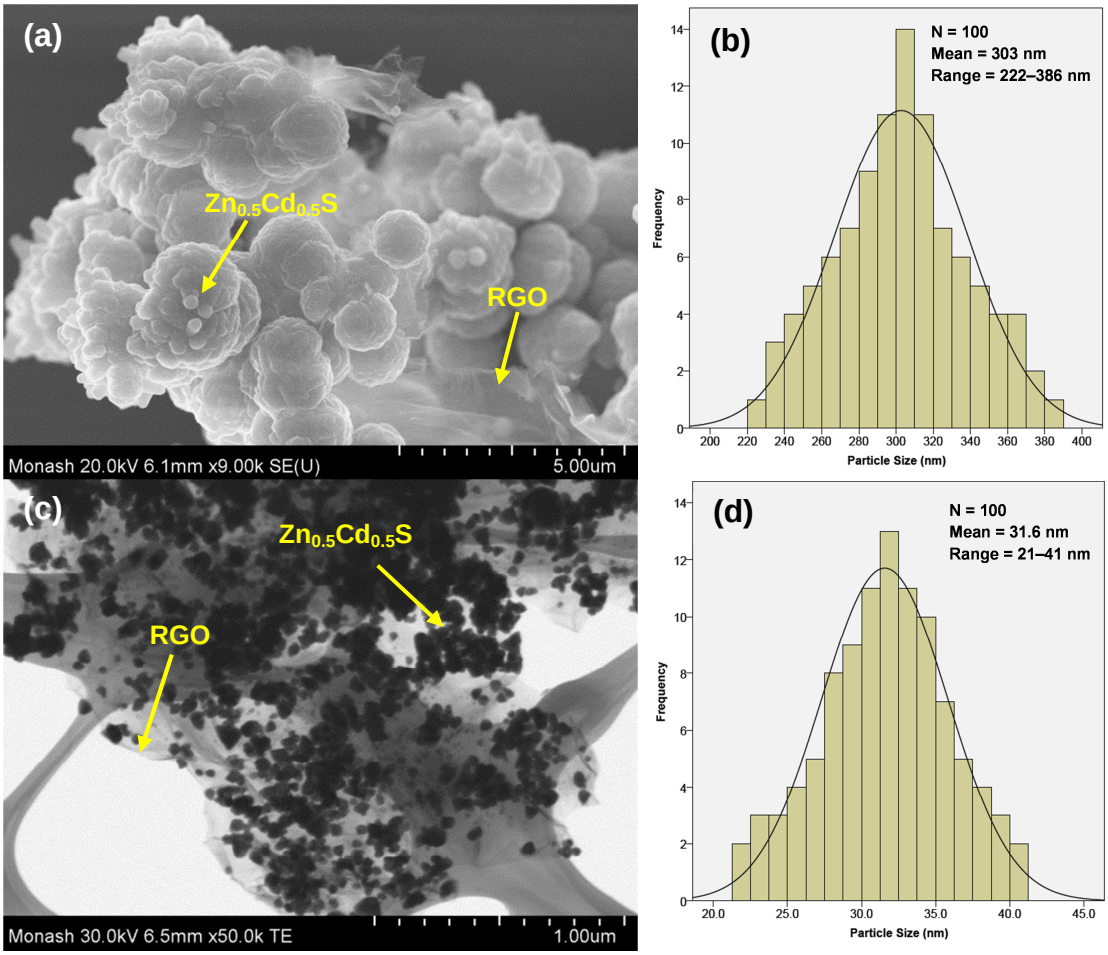

Fig. S3 (a) FESEM image of 20RGO-$Zn_{0.5}Cd_{0.5}S$-H (in the absence of NaOH as a precipitating agent). (b) Particle size distribution of $Zn_{0.5}Cd_{0.5}S$ decorated on RGO sheets without adding NaOH in the reaction medium. (c) STEM image of 20RGO-$Zn_{0.5}Cd_{0.5}S$ (in the presence of NaOH as a precipitating agent). (d) Particle size distribution of $Zn_{0.5}Cd_{0.5}S$ supported on RGO sheets on addition of NaOH in the reaction medium.

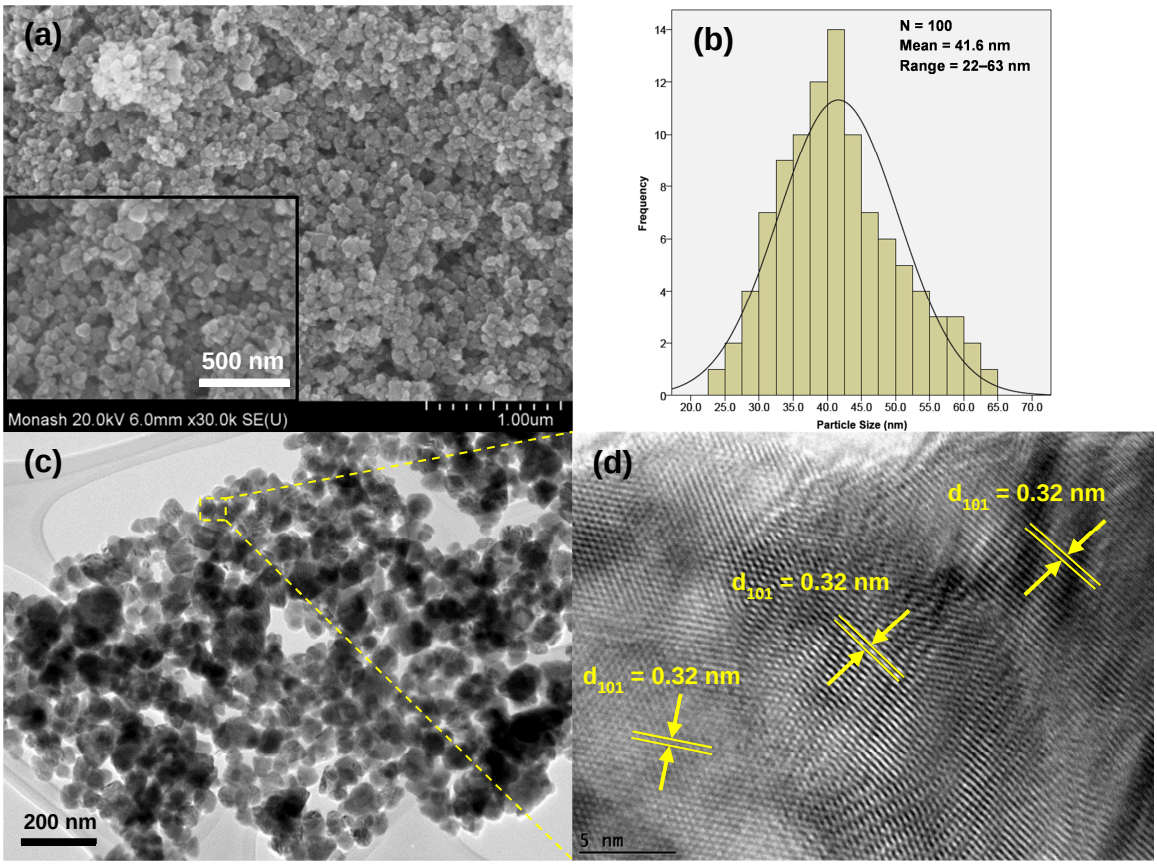

Fig. S4 (a) FESEM image of pristine $Zn_{0.5}Cd_{0.5}S$ (inset shows the magnified FESEM image of pristine $Zn_{0.5}Cd_{0.5}S$. (b) Particle size distribution of pristine $Zn_{0.5}Cd_{0.5}S$ in the absence of RGO. (c) TEM and (d) HRTEM images of pristine $Zn_{0.5}Cd_{0.5}S$.

(4) XRD patterns of the $Zn_xCd_{1-x}S$ nanocomposites

As demonstrated in Fig. S5, all the $Zn_xCd_{1-x}S$ nanocomposites exhibited an apparent shift in the XRD patterns. It is observed that the diffraction peaks for all the studied samples presented an obvious shift towards the higher angles from CdS (JCPDS 41-1049) to ZnS (JCPDS 5-0566) with increasing Zn content. This clearly inferred that the as-synthesized solid solution of $Zn_xCd_{1-x}S$ samples was formed instead of a simple mixture of ZnS and CdS crystals, which agreed well with the literatures.[3] The successful formation of $Zn_xCd_{1-x}S$ solid solution was owing to the fact that the smaller ionic radius of Zn^{2+} ion could be incorporated into the lattice of CdS crystals.[4,5] Evidently, the ionic radius of Zn^{2+} ion (0.74 Å) was smaller than that of Cd^{2+} (0.97 Å).[6] More importantly, the similar electronegativity of both Zn (1.65) and Cd (1.69) was also advantageous to produce the $Zn_xCd_{1-x}S$ solid solution.[7]

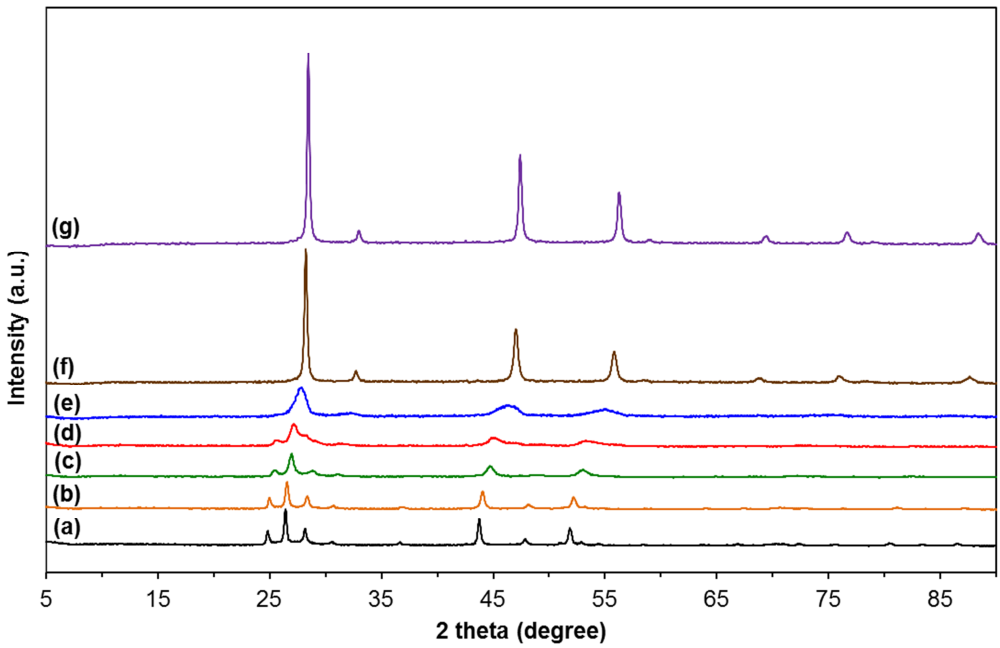

Fig. S5 XRD patterns of (a) CdS, (b) $Zn_{0.1}Cd_{0.9}S$, (c) $Zn_{0.3}Cd_{0.7}S$, (d) $Zn_{0.5}Cd_{0.5}S$, (e) $Zn_{0.7}Cd_{0.3}S$, (f) $Zn_{0.9}Cd_{0.1}S$ and (g) ZnS.

(5) XRD patterns of the RGO-based photocatalysts as control experiments

By comparing 20RGO-$Zn_{0.5}Cd_{0.5}S$ with 20RGO-ZnS and 20RGO-CdS, all these nanocomposites demonstrated an apparent shift in the XRD patterns (Fig. S6). When Zn was incorporated into the CdS crystal, the diffraction peaks of 20RGO-$Zn_{0.5}Cd_{0.5}S$ presented an obvious shift towards the higher angle. This implied that Zn^{2+} incorporated into the lattice of CdS crystal and decreased the fringe lattice distance of the CdS due to smaller radius of Zn^{2+} ion (0.74 Å) than that of Cd^{2+} (0.97 Å).[4,5] The XRD patterns of 20RGO-CdS and 20RGO-ZnS matched well with the standard spectra of pure CdS and ZnS (JCPDS 41-1049 and 5-0566, respectively). The lattice constants *a* and *c* for cubic phase of 20RGO-ZnS and hexagonal phase of 20RGO-CdS and 20RGO-$Zn_{0.5}Cd_{0.5}S$ solid solutions were calculated using eqn (1)–(2), respectively.[8]

$$\frac{1}{d^2} = \frac{h^2+k^2+l^2}{a^2} \quad (1)$$

$$\frac{1}{d^2} = \frac{4}{3}\left(\frac{h^2+hk+k^2}{a^2}\right) + \frac{l^2}{c^2} \quad (2)$$

The calculated lattice constants *a* and *c* of 20RGO-ZnS, 20RGO-$Zn_{0.5}Cd_{0.5}S$ and 20RGO-CdS are summarized in Table S1. The changes in lattice constants for these nanocomposites proved that a solid solution of $Zn_{0.5}Cd_{0.5}S$ was formed instead of physical coupling between ZnS and CdS crystals.

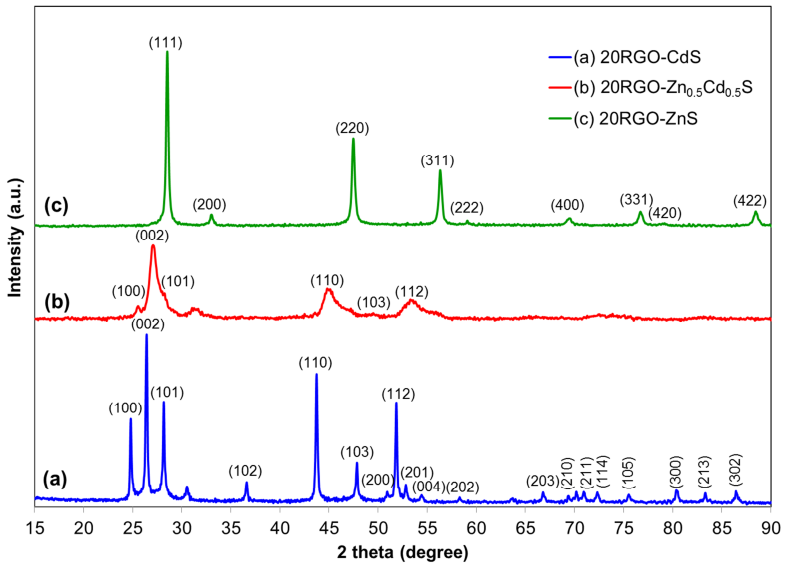

Fig. S6 XRD patterns of (a) 20RGO-CdS, (b) 20RGO-$Zn_{0.5}Cd_{0.5}S$ and (c) 20RGO-ZnS nanocomposites.

Table S1 The lattice constants of 20RGO-CdS, 20RGO-$Zn_{0.5}Cd_{0.5}S$ and 20RGO-ZnS nanocomposites.

Photocatalyst	20RGO-CdS	20RGO-$Zn_{0.5}Cd_{0.5}S$	20RGO-ZnS
Lattice constant, *a* (Å)	4.1409	4.0205	5.406
Lattice constant, *c* (Å)	6.7198	6.5812	5.406

(6) Adsorption-desorption equilibrium of RB5 on the photocatalysts in the dark

From Fig. S7, it could be shown that the adsorption-desorption equilibrium of RB5 was attained within 30 min in the dark. Apparently, the adsorptivity of RB5 molecules on the 20RGO-$Zn_{0.5}Cd_{0.5}S$ was greater than that on the pristine $Zn_{0.5}Cd_{0.5}S$ owing to the hybridization of $Zn_{0.5}Cd_{0.5}S$ with RGO. The addition of RGO was found to enhance the adsorptivity of RB5 *via* π-π conjugation between RB5 and aromatic regions of RGO.[9]

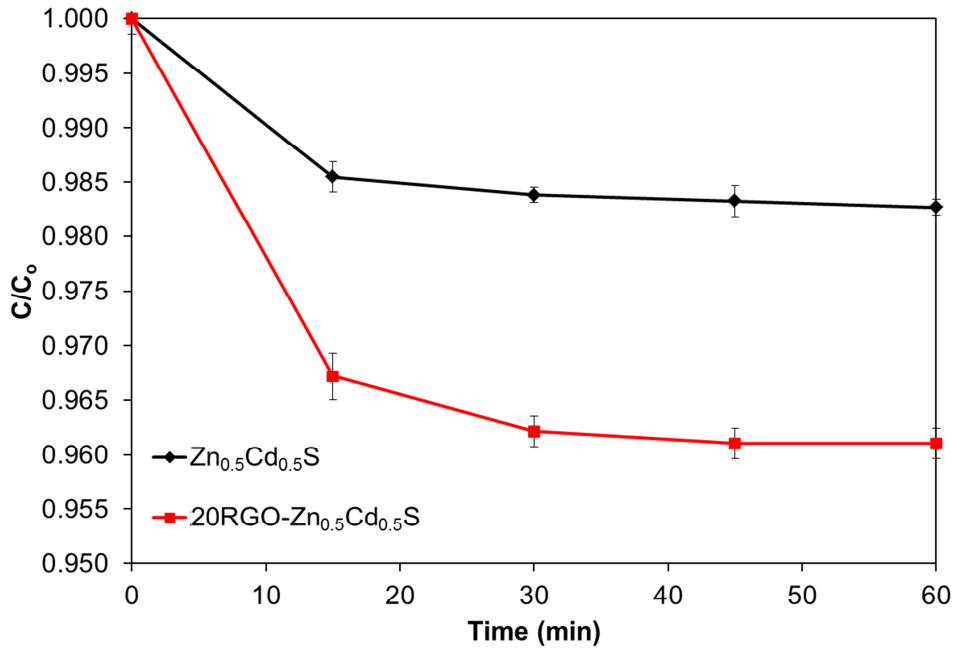

Fig. S7 The adsorption-desorption equilibrium of RB5 on the pristine $Zn_{0.5}Cd_{0.5}S$ and 20RGO-$Zn_{0.5}Cd_{0.5}S$ nanocomposites in the dark.

(7) Electronegativity calculation method for the electronic band structure of $Zn_{0.5}Cd_{0.5}S$ using Mulliken electronegativity theory

The conduction band (CB) edge energy of $Zn_{0.5}Cd_{0.5}S$ was estimated using Mulliken electronegativity theory.[3,10] The CB and valence band (VB) potentials of the semiconductors at the point of zero charge were calculated by the following equation:[11]

$$E_{CB} = \chi - E^e - 0.5E_g \quad (3)$$

Herein, E_{CB} is the CB edge energy. The χ is the absolute electronegativity of the semiconductor, which is defined as the geometric mean of the electronegativity of the constituent atoms. The χ value for $Zn_{0.5}Cd_{0.5}S$ was calculated to be 5.345 eV. For a typical $Zn_xCd_yS_z$, the χ value was determined using eqn (4)–(7).[4]

$$\chi = (\chi_{Zn}^x \times \chi_{Cd}^y \times \chi_S^z)^{\frac{1}{x+y+z}} \quad (4)$$

$$\chi_{Zn} = \frac{1}{2}(A_{Zn} + I_{Zn}) \quad (5)$$

$$\chi_{Cd} = \frac{1}{2}(A_{Cd} + I_{Cd}) \quad (6)$$

$$\chi_S = \frac{1}{2}(A_S + I_S) \quad (7)$$

E^e is the energy of free electrons on the hydrogen scale (*ca*. 4.5 eV). E_g is the band gap energy of the semiconductor obtained from the UV-Vis diffuse reflectance spectroscopy. The VB edge energy was obtained by $E_{VB} = E_{CB} + E_g$. From the calculation, the E_{CB} and E_{VB} values of $Zn_{0.5}Cd_{0.5}S$ were estimated to be –0.42 eV and 2.11 eV respectively.

References

1 W. S. Hummers and R. E. Offeman, *J. Am. Chem. Soc.*, 1958, **80**, 1339-1339.
2 Y. Zhang, Z.-R. Tang, X. Fu and Y.-J. Xu, *ACS Nano*, 2011, **5**, 7426-7435.
3 Q. Li, H. Meng, P. Zhou, Y. Zheng, J. Wang, J. Yu and J. Gong, *ACS Catal.*, 2013, **3**, 882-889.
4 C.-C. Chan, C.-C. Chang, C.-H. Hsu, Y.-C. Weng, K.-Y. Chen, H.-H. Lin, W.-C. Huang and S.-F. Cheng, *Int. J. Hydrogen Energy*, 2014, **39**, 1630-1639.
5 Y. Wang, J. Wu, J. Zheng and R. Xu, *Catal. Sci. Technol.*, 2011, **1**, 940-947.
6 S. N. Garaje, S. K. Apte, S. D. Naik, J. D. Ambekar, R. S. Sonawane, M. V. Kulkarni, A. Vinu and B. B. Kale, *Environ. Sci. Technol.*, 2013, **47**, 6664-6672.
7 X. Wang, H. Tian, X. Cui, W. Zheng and Y. Liu, *Dalton Trans.*, 2014, **43**, 12894-12903.

8 J. Wang, B. Li, J. Chen, L. Li, J. Zhao and Z. Zhu, *J. Alloys Compd.*, 2013, **578**, 571-576.
9 Z. Chen, N. Zhang and Y.-J. Xu, *CrystEngComm*, 2013, **15**, 3022-3030.
10 J. Zhang, L. Qi, J. Ran, J. Yu and S. Z. Qiao, *Adv. Energy Mater.*, 2014, **4**, 1301925.
11 C. Yu, G. Li, S. Kumar, K. Yang and R. Jin, *Adv. Mater.*, 2014, **26**, 892-898.